Inorg. Chem. **2007**, *46*, 3475–3484

Rare Earth Arenedisulfonate Metal–Organic Frameworks: An Approach toward Polyhedral Diversity and Variety of Functional Compounds

Felipe Gándara, Alberto García-Cortés, Concepción Cascales, Berta Gómez-Lor, Enrique Gutiérrez-Puebla, Marta Iglesias, Angeles Monge,* and Natalia Snejko

Instituto de Ciencia de Materiales de Madrid, CSIC, Cantoblanco, E-28049 Madrid, Spain

Received September 18, 2006

Eight 2D and 3D metal–organic framework (MOF) rare earth naphthalenedisulfonates have been obtained. The different geometry of the naphthalenedisulfonic acids used as connectors [(1,5-NDS) and (2,6-NDS)] gives rise to the three new structure types. In $Ln(OH)(1,5\text{-NDS})H_2O$, LnPF-1 (lanthanide polymeric framework; Ln = La, Nd, Pr, Sm and Eu), the lanthanide ion is octacoordinated. Its 3D structure is formed by (Ln_2O_{14})–S–(Ln_2O_{14}) infinite chains, connected through complete NDS connectors. LnPF-2 (Ln = Nd), with the same empirical formula as the former, and the lanthanide in octa- and nonacoordination, owns an arrangement of sulfonate bridges and neodymium polyhedra that gives rise to a 2D structure. $[Ln_5(2,6\text{-NDS})_3(OH)_9(H_2O)_4](H_2O)_2$, LnPF-3 (Ln = Nd, Eu), demonstrates that it is possible to obtain a 3D structure with (2,6-NDS), when a greater Ln/connector ratio is employed. It is worth pointing out the existence, in this latter family of compounds, of a μ^5-OH group, whose hydrogen atom is very close to one-sixth Ln atom (distance Ln···H = 2.09 Å). The materials, with high thermal stability, act as active and selective bifunctional heterogeneous catalysts in oxidation of linalool yielding cyclic hydroxy ethers. The absence of any 3D Nd–Nd magnetic interaction is explained due to the inner nature of 4f orbitals of Nd^{3+}, which do not favor the magnetic exchange. The influence of the polymeric frame matrix results in a better photoluminescence efficiency for NdPF-1.

Introduction

Current efforts on hybrid metal−organic complexes are directed mostly toward synthesis of diverse frameworks using polycarboxylates[1−4] and phosphonates.[5] Many fewer studies are, however, dedicated to polymeric organo-inorganic sulfonates, in spite of the fact that the sulfonic group, being regarded typically as weakly coordinating,[6] shows, in a properly planned synthesis, a pronounced effect on the appropriately chosen metal center. The supramolecular chemistry of the sulfonate group in extended solids has been reviewed by Côte and Shimizu,[7] and that of the metal arene sulfonates, by J. Cai.[8] Structures of compounds of group 1 and 2 metal ions with 1,5-NDS are also found.[9] Mix Ln-sulfonate−phosphonates[10] and an interesting structural study on lanthanide−sulfoisophtalic coordination polymers[11]

* Corresponding author. E-mail: amonge@icmm.csic.es.

(1) (a) Perles, J.; Iglesias, M.; Martín Luengo, M. A.; Monge, M. A.; Ruiz-Valero, C.; Snejko, N. *Chem. Mater.* **2005**, *17*, 5837. (b) Gómez-Lor, B.; Gutiérrez-Puebla, E.; Iglesias, M.; Monge, A.; Ruiz-Valero, C.; Snejko, N. *Chem. Mater.* **2005**, *17*, 2568. (c) Monge, A.; Snejko, N.; Gutiérrez-Puebla, E.; Medina, M.; Ruiz-Valero, C.; Iglesias, M.; Gómez- Lor, B. *Chem. Commun.* **2005**, *10*, 1291.

(2) (a) Tamaki, H.; Zhong, Z. J.; Matsumoto, N.; Kida, S.; Koikawa, K.; Achiwa, N.; Okawa, H. *J. Am. Chem. Soc.* **1992**, *114*, 6974. (b) Mathoniere, C.; Nuttall, C. J.; Carling, S. G.; Day, P. *Inorg. Chem.* **1996**, *35*, 1201. (c) Decurtins, S.; Schmalle, H. W.; Schneuwly, P.; Ensling, J.; Gütlich, P. *J. Am. Chem. Soc.* **1994**, *116*, 9521. (d) Andrés, R.; Brissard, M.; Gruselle, M.; Train, C.; Vaissermann, J.; Malezieux, B. N.; Jamet, J. P.; Verdaguer, M. *Inorg. Chem.* **2001**, *40*, 4633.

(3) (a) Deakin, L.; Ariff, A. H.; Miller, J. S. *Inorg. Chem.* **1999**, *38*, 5072. (b) Lo, M. F. S.; Chui, S. Y. S.; Shek, L. Y.; Liu, Z.; Zhang, X. X.; Wen, G. H.; Willams, I. D. *J. Am. Chem. Soc.* **2000**, *122*, 6293.

(4) Chui, S. Y. S.; Lo, S. M. F.; Charmant, J. P. H.; Orpen, A. G.; Willams, I. D. *Science* **1999**, *238*, 1148.

(5) (a) Clearfield, A. *Prog. Inorg. Chem.* **1998**, *47*, 371. (b) Mallouk, T. E.; Garvin, J. A. *Acc. Chem Res.* **1998**, *31*, 209. (c) Byrd, H.; Clearfield, A.; Poojary, D.; Reis, K. P.; Thompson, M. E. *Chem. Mater.* **1996**, *8*, 2239. (d) Vermeulen, L. A.; Snover, J. L.; Sapochak, L. S.; Thompson, M. E. *J. Am. Chem. Soc.* **1993**, *115*, 11767. (e) Kumar, C. V.; Chauduri, A. *Chem. Mater.* **2001**, *13*, 238. (f) Alberti, G.; Constantino, U.; Marmottini, F.; Vivan, R.; Zapelli, P. *Angew. Chem., Int. Ed. Engl.* **1993**, *32*, 1357. (g) Sun, Z. M.; Mao, J. G.; Sun, Y. Q. et al. *New J. Chem.* **2003**, *27*, 1326. (h) Rao, K. P.; Balraj, V.; Minimol, M. P. et al. *Inorg. Chem.* **2004**, *43*, 2004. (i) Maeda, K. *Microporous Mesoporous Mater.* **2004**, *73* (1−2), 47. (k) Song, S. Y.; Ma, J. F.; Yang, J. et al. *Inorg. Chem.* **2005**, *44*, 2140.

(6) Lawrance, G. A. *Chem. Rev.* **1986**, *86*, 17.

(7) Côte, A. P.; Shimizu. *Coord. Chem. Rev.* **2003**, *86*, 17.

(8) Cai, J. *Coord. Chem. Rev.* **2004**, *248*, 1061 and references therein.

(9) Cai, J. W.; Chen, C. H.; Liao, C. Z.; Feng, X. L.; Chen, X. M. *Acta Crystallogr., Sect. B* **2001**, *57*, 520.

(10) Song, J.-l.; Lei, C.; Mao, J. G. *Inorg. Chem.* **2004**, *43*, 5630.

10.1021/ic0617689 CCC: $37.00
Published on Web 04/04/2007

Table 1. Main Crystallographic Data for LnPF-1 Structure Type (L = 1,5-NDS) and for LnPF-2 and LnPF-3 Structure Type (L = 2,6-NDS) Compounds

	$NdL(OH)(H_2O)$ (LnPF-1)	$LaL(OH)(H_2O)$ (LnPF-1)	$EuL(OH)(H_2O)$ (LnPF-1)	$[NdL(OH)(H_2O)]_4$ (LnPF-2)	$[Nd_{2.5}L_{1.5}(OH)_{4.5}(H_2O)_2](H_2O)$ (LnPF-3)	$[Eu_{2.5}L_{1.5}(OH)_{4.5}(H_2O)_2](H_2O)$ (LnPF-3)
empirical formula	$C_{10}H_9NdO_8S_2$	$C_{10}H_9LaO_8S_2$	$C_{10}H_9EuO_8S_2$	$C_{40}H_{36}Nd_4O_{32}S_8$	$C_{15}H_{19.5}Nd_{2.5}O_{16.5}S_3$	$C_{15}H_{19.5}Eu_{2.5}O_{16.5}S_3$
fw	465.53	460.20	473.25	1862.13	920.59	939.89
cryst syst	triclinic	triclinic	triclinic	monoclinic	monoclinic	monoclinic
space group	*P*1	*P*1	*P*1	Cc	*C*2/*c*	*C*2/*c*
a (Å)	5.6745(8)	5.7263(2)	5.6309(3)	19.510(1)	34.228(4)	33.933(1)
b (Å)	10.551(2)	10.6104(4)	10.5165(5)	10.559(8)	5.9374(7)	5.857(2)
c (Å)	11.450(2)	11.5533(5)	11.3974(5)	25.340(2)	24.332(3)	24.148(1)
α (deg)	76.456(2)	76.615(1)	76.320(1)	90	90	90
β (deg)	77.484(2)	77.619(1)	77.351(1)	98.448(1)	110.395(2)	110.237(1)
γ (deg)	88.034(2)	87.937(1)	88.063(1)	90	90	90
Z	2	2	2	4	8	8
V (Å^3)	650.5(2)	666.94(4)	639.74(5)	5163.9(7)	4634.9(9)	4503.1(3)
density (calcd mg/m^3)	2.377	2.292	2.457	2.395	2.639	2.773
abs coeff (mm^{-1})	4.349	3.552	5.266	4.383	5.880	7.251
F (000)	450	444	456	3600	3516	3576
cryst size (mm^3)	0.2 × 0.2 × 0.06	0.16 × 0.16 × 0.16	0.20 × 0.16 × 0.06	0.30 × 0.20 × 0.10	0.10 × 0.07 × 0.05	0.20 × 0.20 × 0.10
θ for data collection	3.75−30.98°	1.85−29.51°	1.88−26.37°	1.62−28.93°	1.27−29.07°	1.27−26.37°
index range	(8, 14, 16) (−8, −9, −14)	(7, 14, 15) (−7, −14, −15)	(7, 13, 14) (−6, −12, −14)	(25, 14, 34) (−26, −14, −33)	(45, 7, 32) (−44, −7, −33)	(42, 7, 30) (−40, −7, −30)
reflns collected	4574	7738	5030	22606	20084	16182
unique reflns	3420 [R_{int} = 0.057]	3375 [R_{int} = 0.039]	2407 [R_{int} = 0.027]	11619 [R_{int} = 0.047]	5744 (R_{int} = 0.0417)	4558 (R_{int} = 0.0604)
GOF on F^2	0.799	0.813	1.203	0.993	1.192	1.149
R indices	R1 = 0.05	R1 = 0.034	R1 = 0.049	R1 = 0.0406	R1 = 0.0546	R1 = 0.062
[$I > 2\sigma(I)$]	wR2 = 0.12	wR2 = 0.071	wR2 = 0.13	wR2 = 0.0823	wR2 = 0.1203	wR2 = 0.100
R indices	R1 = 0.09	R1 = 0.044	R1 = 0.057	R1 = 0.0557	R1 = 0.0747	R1 = 0.091
(all data)	wR2 = 0.13	wR2 = 0.075	wR2 = 0.13	wR2 = 0.0866	wR2 = 0.1354	wR2 = 0.109
max diff peak and hole (e Å^{-3})	2.27 and −1.87	1.25 and −1.16	2.472 and −2.73	2.743 and −1.229	1.669 and −2.941	1.239 and −1.457

have been recently reported. Of special interest are metal−organic frameworks constructed from carefully selected arenedisulfonates and rare earth elements; surprisingly, there are only a couple of structural reports on disulfonate coordination compounds, with both sulfonate groups coordinated to the rare earth ions, one of them with mixed ligands,[12] and the other reported in a communication by our group.[13] In our ongoing studies of arene−sulfonate groups[14,15] as linkers in the search of multifunctional materials, we report here eight novel two- and three-dimensional Ln^{3+}−organic frameworks belonging to three different structural types, in which the metal centers are coordinated to 1,5- and 2,6-naphthalenedisulfonate (NDS^{2-}) ligands. Regarding the properties, the aim of this paper is to perform a comparative study of catalytic, magnetic, and optical characteristics for some representatives, and their relationship with the three structural types. This study can be understood as a starting point to tune the required properties with the structural features of new purely disulfonate MOFs, taking into account that these latter species are tailored through the used synthetic conditions.

Experimental Section

General Information. All reagents were purchased at high purity (AR grade) from Aldrich and used without further purification. The IR spectra were recorded from KBr pellets in the range 4000−400 cm^{-1} on a Perkin-Elmer spectrometer. Thermogravimetric and differential thermal analyses (TGA-DTA) were performed using a SEIKO TG/DTA 320 apparatus in the temperature range between 25 and 700 °C in N_2 (flow of 50 mL/min) atmosphere and at a heating rate of 5 °C/min.

Synthesis. Ln(OH)(1,5-NDS)H_2O (Ln = La, Nd, Pr, Sm, Eu), LnPF-1. 1,5-NDS (1,5-naphthalenedisulfonate) and $[Ln_5(2,6\text{-NDS})_3(OH)_9(H_2O)_4](H_2O)_2]$ (Ln = Nd, Eu), LnPF-3 (2,6-NDS = 2,6-naphthalenedisulfonate), were obtained by treating an aqueous solution containing a mixture of equimolar amounts of the corresponding $Ln(NO_3)_3{\cdot}6H_2O$ and Na_2(1,5-NDS) or Na_2(2,6-NDS) in 7 mL of water under hydrothermal reaction conditions (24 h, 170 °C). LnPF-3 synthesis was repeated further (after knowing its composition) in a 5:3 Ln/Na_2(2,6-NDS) ratio, obtaining, as expected, the compound with a higher yield. The synthesis of Nd(OH)(2,6-NDS)H_2O(LnPF-2) was carried out by reaction of $Nd(NO_3)_3{\cdot}6H_2O$, Na_2(2,6-NDS), and 4,4′-bipy or *trans*-1-(2-Py)-2-(4-Py) ethylene (0.82:1:1) in 8 mL of water under hydrothermal reaction conditions (36 h, 180 °C). The organic amines, not being found in the LnPF-2 structure, play a role not only in creating the appropriate pH, but also in introducing a templating effect in the crystallization of this compound. The crystalline products were separated by suction filtration, washed with water, and dried in air, and their purity checked by X-ray powder diffraction by comparison with the simulated patterns on the basis of the single-crystal data.

X-ray Structure Determinations. A summary of the main crystal and refinement data for the three compounds is given in Table 1. Data for single crystals of LnPF-1 (Ln = La, Nd, Eu), LnPF-2 (Ln = Nd), and LnPF-3 (Ln = Nd, Eu) were collected in a Bruker SMART CCD diffractometer equipped with a normal focus, 2.4 kW, sealed tube X-ray source (Mo Kα radiation = 0.71073 Å). Data were collected over a hemisphere of the reciprocal space by a combination of three sets of exposures. Each exposure of 20 s covered 0.3° in ϖ. Unit cell dimensions were determined

(11) Liu, Q.-Y.; Xu, L. *Eur. J. Inorg. Chem.* **2005**, 3458.
(12) Deacon, G. B.; Gitilits, A.; Zelestny, G.; Stellfeldt, D.; Meyer, G. *Z. Anorg. Allg. Chem.* **1999**, *625*, 764.
(13) Snejko, N.; Cascales, C.; Gomez-Lor, B.; Gutiérrez-Puebla, E.; Iglesias, M.; Ruiz-Valero, C.; Monge, M. A. *Chem. Commun.* **2002**, 1366.
(14) Gándara, F.; Fortes-Revilla, C.; Snejko, N.; Gutiérrez-Puebla, E.; Iglesias, M.; Monge. M. A. *Inorg. Chem.*, in press.
(15) Gándara, F.; Perles, P.; Snejko, N.; Iglesias, M.; Gómez-Lor, B.; Gutiérrez-Puebla, E.; M. Monge, M. A. *Angew. Chem., Int. Ed.*, in press.

by a least-squares fit of 60 reflections with $I > 20\sigma(I)$. The structures were solved by direct methods. Coordinated water molecules in LnPF-3 split into two very close positions; this small disorder is absorbed by the thermal parameter of their oxygen atoms. The final cycles of refinement were carried out by full-matrix least-squares analyses with anisotropic thermal parameters for all non-hydrogen atoms. Hydrogen atoms of the hydroxyl groups and water molecules were located in difference Fourier maps. Calculations were carried out with SMART software for data collection and data reduction and SHELXTL.[16] CCDC reference numbers 182916, 182917, 298197, 298198, 298199, and 298200 contain the supplementary crystallographic data for this paper. These data can be obtained free of charge from the Cambridge Crystallographic Data Center, 12 Union Road Cambridge CB21EZ, U.K. Fax: (−44)-1223-336-033. E-mail:deposit@ccdc.cam.ac.uk.

Catalytic Experiments. The oxidation of linalool was carried out in a batch reactor at atmospheric pressure, 343 K, using acetonitrile as solvent (5 mL). A 0.01 mmol portion of the catalyst (previously homogenized by milling in an agate mortar) was stirred in a suspension containing the solvent and 1.0 mmol of the allylic alcohol. The oxidant (H_2O_2, 30%, 3 mmol) was added dropwise, while the overall suspension was heated up to 343 K. Samples were taken at regular times and analyzed by gas chromatography.

Physical Measurements. A Quantum Design XL-MPMS superconducting quantum interference device SQUID magnetometer operating in the temperature range 2−300K at 1000 Oe was used to perform the magnetic susceptibility measurements for the three magnetic samples. Diamagnetic corrections were calculated with conventional values.[17] The room-temperature (RT) photoluminescence (PL) spectra of Nd^{3+} in the three hosts LnPF-1, LnPF-2, and LnPF-3 were recorded by exciting the corresponding $^4F_{5/2} + {}^2H_{9/2}$ multiplets (pump level in the four-level Nd-laser scheme) with a continuous wave Ti-sapphire laser, λ_{ex} =796.4, 801.6, and 803 (±0.5 nm), respectively, and collecting the luminescence from $^4F_{3/2}$ to $^4I_{13/2}$ ($\lambda_{em} \approx 1.35$ μm), $^4I_{11/2}$ ($\lambda_{em} \approx 1.06$ μm), and $^4I_{9/2}$. The emission was dispersed with a Spex spectrometer ($f = 34$ cm), and the signal was recorded with a cooled Ge photodiode detector, using the lock-in amplifier technique. The PL was corrected, in each case, by the spectral response of the used equipment. Room-temperature optical absorption measurements were made in a Varian spectrophotometer model CARY 5E. Used samples were thin pellets of the stoichiometric Nd-compounds dispersed either on polyethylene or KBr. Further measurement details can be found elsewhere.[18]

Results and Discussion

LnPF-1. X-ray single crystal data and powder diffraction patterns showed that the five La, Nd, Pr, Sm, and Eu compounds own the same structure type. In Ln(OH)(1,5-NDS)H_2O (LnPF-1), the lanthanide ion is octacoordinated (Table 2, Figure 1) to two μ_2-(OH) groups, one water molecule, and five oxygen atoms of different 1,5-NDS ligands in a LnO_8 triangulated dodecahedron (Figure 2). Every two of these (LnO_8) polyhedra share the (OH)−(OH) edge, giving rise to dimeric units, which are isolated in the *b* direction and joined through S atoms in the *a* direction. Connections along the *c* direction are made via whole 1,5-NDS ligands. Hence, the structure can be thought of as formed by (Ln_2O_{14}) dimers that give rise to (Ln_2O_{14})−S−(Ln_2O_{14}) infinite chains, kept together along the *c* direction through the complete NDS linker. There are two differently coordinated NDS anions, which are perpendicularly oriented along the [$\bar{2}$10] and the [210] directions. One of them coordinates to six distinct Ln atoms in a symmetric $\eta^3\mu^3-\eta^3\mu^3$ mode, whereas the other is bonded only to four lanthanide atoms in $\eta^2\mu^2-\eta^2\mu^2$ way.

Table 2. Coordination and Closest Metal−Metal Distances in LnPF-1, LnPF-2, and LnPf-3 Compounds

LnPF-1	La	Nd	Eu
Ln(1)−O(1)	2.602(5)	2.551(7)	2.498(9)
Ln(1)−O(2)	2.344(3)	2.324(7)	2.314(8)
Ln(1)−O(2)	2.379(4)	2.290(7)	2.258(9)
Ln(1)−O(4)	2.570(3)	2.519(6)	2.477(9)
Ln(1)−O(5)	2.508(3)	2.471(7)	2.414(7)
Ln(1)−O(6)	2.688(3)	2.498(6)	2.446(8)
Ln(1)−O(7)	2.630(3)	2.589(6)	2.546(7)
Ln(1)−O(8)	2.527(3)	2.460(6)	2.429(8)
Ln(1)−Ln(1)	3.883(5)	3.801(1)	3.744(1)

LnPF-2	Nd	LnPF-3	Nd	Eu
Ln(1)−O(2)	2.495(7)	Ln(1)−O(4)	2.429(8)	2.402(9)
Ln(1)−O(6)	2.477(7)	Ln(1)−O(5)	2.475(7)	2.364(1)
Ln(1)−O(14)	2.435(8)	Ln(1)−O(9)	2.415(6)	2.373(9)
Ln(1)−O(16)	2.473(7)	Ln(1)−O(10)	2.403(7)	2.373(8)
Ln(1)−O(19)	2.484(9)	Ln(1)−O(11)	2.68(2)	2.63(2)
Ln(1)−O(25)	2.506(7)	Ln(1)−O(12)	2.675(2)	2.473(7)
Ln(1)−O(26)	2.243(8)	Ln(1)−O(13)	2.399(5)	2.352(7)
Ln(1)−O(31)	2.629(8)	Ln(1)−O(14)	2.427(6)	2.382(7)
Ln(1)−Ln(2)	3.903(1)	Ln(1)−O(15)	2.645(1)	2.584(1)
Ln(2)−O(7)	2.497(7)	Ln(1)−Ln(2)	3.752(1)	3.6824(8)
Ln(2)−O(12)	2.538(7)	Ln(1)−Ln(3)	4.007(1)	3.8598(9)
Ln(2)−O(17)	2.563(8)	Ln(2)−O(1)	2.439(8)	2.386(9)
Ln(2)−O(20)	2.516(7)	Ln(2)−O(2)	2.415(8)	2.365(9)
Ln(2)−O(24)	2.464(7)	Ln(2)−O(7)	2.598(6)	2.570(7)
Ln(2)−O(25)	2.404(8)	Ln(2)−O(9)	2.417(6)	2.389(8)
Ln(2)−O(26)	2.388(6)	Ln(2)−O(10)	2.420(6)	2.384(7)
Ln(2)−O(28)	2.742(7)	Ln(2)−O(13)	2.440(6)	2.395(7)
Ln(2)−O(32)	2.630(8)	Ln(2)−O(14)	2.423(6)	2.385(8)
Ln(3)−O(5)	2.543(8)	Ln(2)−O(15)	2.688(1)	2.637(1)
Ln(3)−O(9)	2.496(7)	Ln(2)−O(17)	2.517(1)	2.494(1)
Ln(3)−O(11)	2.459(7)	Ln(2)−Ln(3)	4.038(1)	3.8912(9)
Ln(3)−O(21)	2.480(7)	Ln(3)−O(9)×2	2.470(6)	2.478(7)
Ln(3)−O(22)	2.453(7)	Ln(3)−O(10)×2	2.518(6)	2.411(7)
Ln(3)−O(27)	2.285(7)	Ln(3)−O(13)×2	2.589(6)	2.585(8)
Ln(3)−O(28)	2.453(7)	Ln(3)−O(14)×2	2.496(6)	2.460(7)
Ln(3)−O(30)	2.480(8)	Ln(3)−O(15)×1	2.77(2)	2.76(2)
Ln(3)−Ln(4)	3.876(1)	Ln(3)···H151[a]	2.09	2.04
Ln(4)−O(3)	2.509(8)	Ln(3)···O(15)[a]	3.161(2)	3.09(2)
Ln(4)−O(4)	2.554(8)	O(15)[a]−H151[a]	1.07	1.05
Ln(4)−O(8)	2.550(9)			
Ln(4)−O(13)	2.436(7)			
Ln(4)−O(18)	2.453(8)			
Ln(4)−O(25)	2.870(7)			
Ln(4)−O(27)	2.337(7)			
Ln(4)−O(28)	2.438(7)			
Ln(4)−O(29)	2.638(9)			

[a] Corresponds to the μ_5-OH group.

LnPF-2. In Nd(OH)(2,6-NDS)H_2O, there are four crystallographically independent neodymium atoms per asymmetric unit. Two of them are octacoordinated to five oxygen atoms of different sulfonate groups, one μ_2-OH, one μ_3-OH, and one water molecule; the other two are nine-coordinated since they share other an extra μ_3-OH (Table 2, Figure 1). In this way, the inorganic part of this framework is formed by two kinds of polyhedra, one of which is a NdO_8 triangulated dodecahedron similar to that of LnPF-1, and the

(16) *Software for the SMART System V5.04 and SHELXTL V 5.1*; Bruker-Siemens Analytical X-ray Instrument Inc.: Madison, WI, 1998.
(17) Boudreaux, E. A.; Mulay, L. N. *Theory and Applications of Molecular Paramagnetism*; Wiley: New York, 1976; p 494.
(18) Cascales, C.; Zaldo, C.; Sáez Puche, R. *Chem. Mater.* **2005**, *17*, 2052.

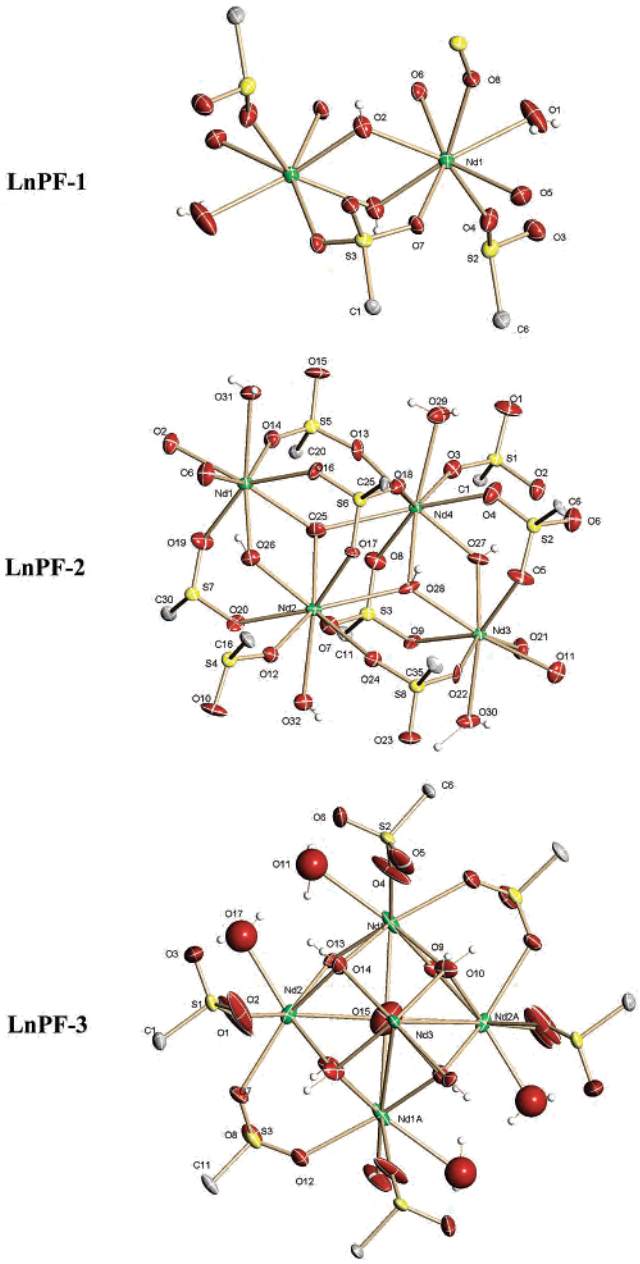

Figure 1. ORTEP view of neodymium clusters.

Figure 2. Coordination polyhedra for the following: (left) LnPF-1 and LnPF-2, LnPF-2 (center), and LnPF-3 (right).

other is a NdO_9 tricapped trigonal prism (Figure 2). Connections among the four polyhedra via μ_2- and μ_3-OH groups lead to tetrameric units. The linkage of these tetramers through sulfonate bridges gives rise to infinite chains along the *b* direction, and through the whole 2,6-NDS connector, to layers perpendicular to the *a* direction. Contrary to what happens in LnPF-1 and in spite of having the same empirical formula, this arrangement results in a 2D structure, undoubtedly due to the geometrical features imposed by the position of the sulfonate groups in the NDS connector. In LnPF-2, each 2,6-NDS ligand is bonded only to four lanthanide atoms, $\eta^2\mu^2-\eta^2\mu^2$, and leaves, thus, two free oxygen atoms.

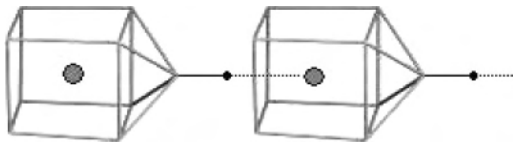

Figure 3. Ln(3)−O(15)−H···Ln(3)−O(15)−H··· sequence in LnPF-3. Black small circle = H atom and gray large circle = Ln(3).

LnPF-3. After several attempts to obtain a 3D framework with 2,6-NDS as linker, crystals of $[Ln_5(2,6\text{-}NDS)_3(OH)_9(H_2O)_4](H_2O)_2$ (Ln = Nd, Eu) were finally obtained. Similarly to LnPF-2, in these compounds the ligand is coordinated in a tetratopic way to the metallic atoms. From the five Ln atoms existing per formula (Figure 1), four [two Ln(1) and two Ln(2)], situated in the middle of $[LnO_3(\mu_3\text{-}OH)_4(\mu_5\text{-}OH)H_2O]$ tricapped trigonal prisms, form $[Ln_4O_{12}(\mu_3\text{–}OH)_8(\mu_5\text{–}OH)(H_2O)_4]$ tetrameric units via hydroxyl groups sharing edges, and the other (Ln3), in a $Ln(\mu_3\text{-}OH)_8(\mu_5\text{-}OH)$ monocapped tetragonal prism (Figure 2), perfectly fits into the tetrameric units by sharing its four triangular faces, giving rise to $[Ln_5O_{12}(\mu_3\text{-}OH)_8(\mu_5\text{-}OH)(H_2O)_4]$ pentameric clusters (Figure 4). Unions of these clusters through the μ_3-OH vertex give rise to backbonelike chains, inside of which (μ_5-OH) hydrogen atoms remain encapsulated. In this manner, a row of Ln(3)−O(15)−H···Ln(3)−O(15)−H··· runs in a straight line inside the chains (Figures 3 and 4). The distance[19] Ln(3)···H(15), being 2.09 and 2.04 Å for Nd and Eu, respectively, could be considered to correspond to a tenth position when considering the Ln(3) polyhedron as a (LnO_9H) bycapped tetragonal prism (Table 2, Figure 3). Very scarce in hybrid solids, this special coordination is encountered, and although a couple of papers with linkage of truncated rare earth $Ln_6-\mu_6O$ clusters have been reported,[20] the inorganic network of LnPF-3, reminiscent of those, seems to be unique due to the ($Ln_5-\mu_5$-O−H−$Ln_5-\mu_5$-O−H···) linkage. Structurally speaking, this kind of association is quite similar to that found in some purely inorganic structures, for instance $Ln_8Ba_5Ni_4O_{21}$,[21] where inside the similar lanthanide pentameric units the central row is formed by a BaO_{10} bicapped tetragonal prism in a Ba−O−Ba−O··· sequence instead of that Ln−O−H···Ln of the current compound.

The $[Ln_5O_{12}(\mu_3\text{-}OH)_8(\mu_5\text{-}OH)(H_2O)_4]_\infty$ backbone chains are connected to each other through the complete linker along the *c* direction (Figure 4).

(19) Evans, W. J.; Greci, M. A.; Séller, J. W. *Inorg. Chem.* **2000**, *39*, 3123. Thomson, M. K.; Lough, A. J.; White, A. J. P.; Williams, D. J.; Kahwa, A. J. G. *Inorg. Chem.* **2003**, *42*, 4828. Blake, A. J.; Gould, R. O.; Craig; Grant, C. M.; Milne, P. E. Y.; Parsons, S.; Winpenny, R. E. P. *J. Chem. Soc., Dalton Trans.* **1997**, 485.
(20) Wang, R.; Carducci, M. D. *Inorg. Chem.* **2000**, 39, 1836. Serre, C.; Pelle, F; Gardant, N.; Ferey, G. *Chem. Mater.* **2004**, *16*, 1177.
(21) (a) Campá, J. A.; Gutiérrez-Puebla, E.; Monge, M. A.; Rasines, I.; Ruiz-Valero, C. *J. Solid State Chem.* **1996**, *126*, 27. (b) Gutiérrez-Puebla, E.; Monge, M. A.; Ruiz-Valero, C.; Campá, J. A. *Chem. Mater.* **1998**, *10*, 3405.

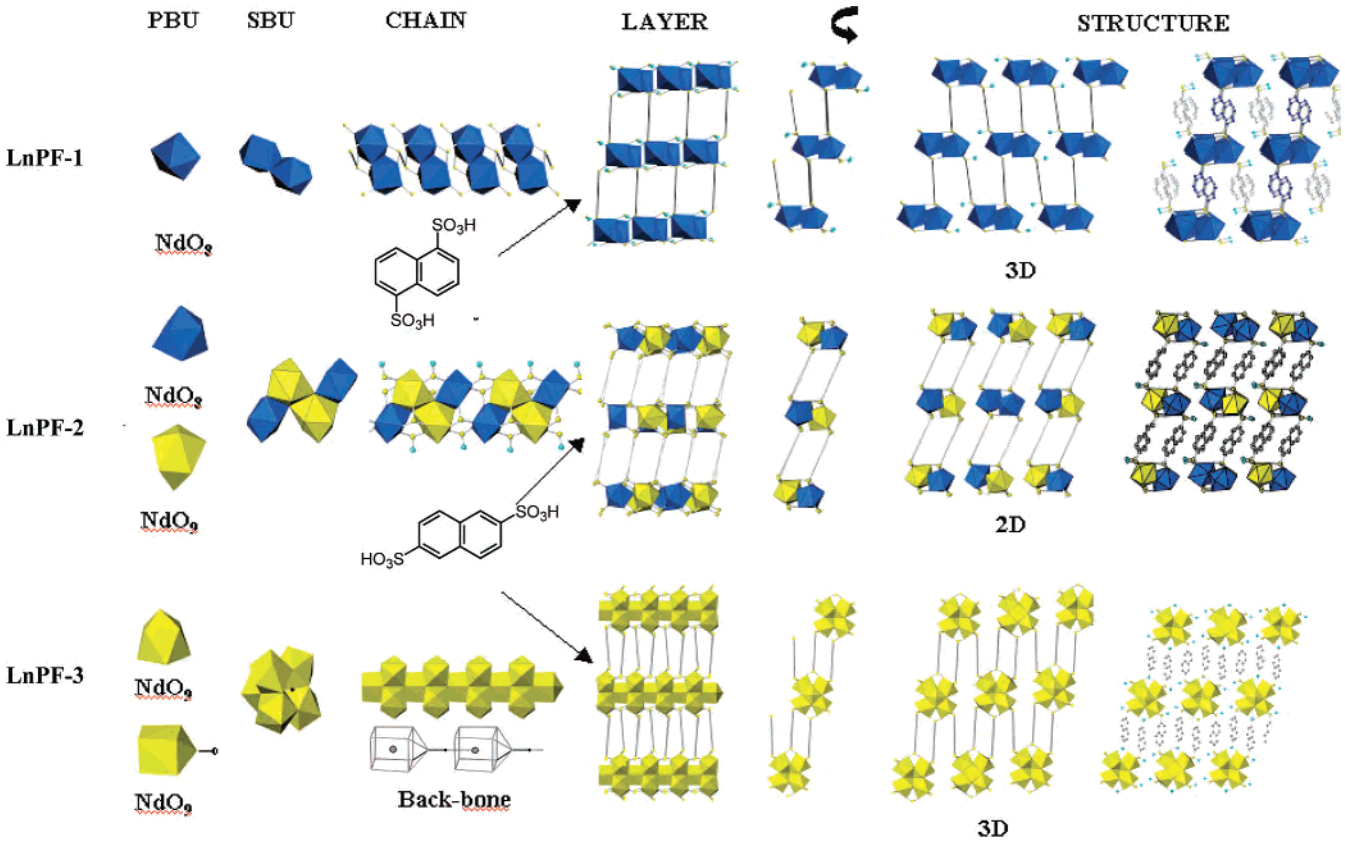

Figure 4. Comparative structural display for LnL(OH)(H_2O) **(**LnPF-1), NdL(OH)(H_2O) **(**LnPF-2), and [$Ln_{2,5}L_{1,5}(OH)_{4,5}(H_2O)_2$]($H_2O$) **(**LnPF-3**)**.

Although all hydrogen atoms were located in Fourier synthesis, concerning that of the μ_5-OH group, whose electron density in the Fourier map could be masked by that of the five plus one surrounding Ln atoms, some extra verification was accomplished as follows. Since the only two possibilities to maintain the compound's electrical neutrality are either the oxygen belonging to one OH group, or its position being partially occupied (only one-half), refinements of the O15 with a population factor of 0.5 were performed. The results led to thermal parameters that were very low or even negative for this atom. This fact together with the synthesis media and the ability of lanthanide to coordinate μ_n hydroxyl groups clearly confirms the formation of the [O(15)−H] hydroxyl groups.

IR spectra of LnPF-1, LnPF-2, and LnPF-3 are very similar and indicate both ν_{as} and ν_s of the SO_3 groups found at 1240−1180 (ν_{as}) and 1100−1040 (ν_s) cm^{-1}, the aromatic C−H stretching mode being situated in the area of 3100−2860 cm^{-1}. The IR spectra of these compounds show additional bands at ca. 3600, 3500−3100, and 1530 cm^{-1}, which correspond to the hydroxy groups and water molecules, respectively.

TG-DTA analysis results for the thermal decomposition of LnPF-1, LnPF-2, and LnPF-3 reveal that their frameworks are stable up to 510 °C (LnPF-1 and LnPF-3) and 550 °C (LnPF-2); above these temperatures the frameworks decompose completely.

For LnPF-1, a weight loss occurs between 240 and 310 °C, accompanied by an endothermic effect corresponding to the loss of the coordinated water molecule per formula unit (calculated, 1.9%; found, 2% for NdPF-1). For LnPF-2, the loss of the four water molecules (calculated, 5.69%; found, 5.92%) occurs between 240 and 500 °C. LnPF-3 loses the water molecules in two steps, the first from 90 to 230 °C followed by a second step (240−500°). The exceptional thermal stability is to be emphasized (in all cases more than 500 °C) for all MOF compounds.

Catalytic Properties. Linalool oxides are extensively found in nature and are mainly used in perfumery and as fragrances. In addition, they seem to have a strong biological significance in certain pollination systems acting as insect attractants.[22] They are obtained usually by extraction from natural products, generally fruits or plants, or by transformation of linalool, but also numerous multistep organic syntheses of pyranoid and furanoid linalool oxides have been reported,[23] some of them highly stereoselective.[24] Oxidation of linalool to the corresponding cyclic hydroxy ethers has been achieved previously by some of us using microporous bifunctional titanium−aluminosilicates catalysts.[25] As the compounds here presented their own both redox and acid sites, the bifunctional character of these materials as catalysts for the transformation of linalool has been tested. The small size of the pore in these structures avoids the accessibility

(22) Borg-Karlson, A.-K.; Unelius, C. R.; Valterova, I.; Nilsson, L. A. *Phytochemistry* **1996**, *41*, 1477.
(23) Fournier-Nguefack, Ch.; Lhoste, P.; Sinou, D. *Tetrahedron* **1997**, *53*, 4353 and references therein.
(24) (a) Vidari, G.; Di Rosa, A.; Zanoni, G.; Bicchi, C. *Tetrahedron: Asymmetry* **1999**, *10*, 3547. (b) Vidari, G.; Di Rosa, A.; Castronovo, F.; Zanoni, G. *Tetrahedron: Asymmetry* **2000**, *11*, 981.
(25) Corma, A.; Iglesias, M.; Sánchez, F. *Chem. Commun.* **1995**, 1635.

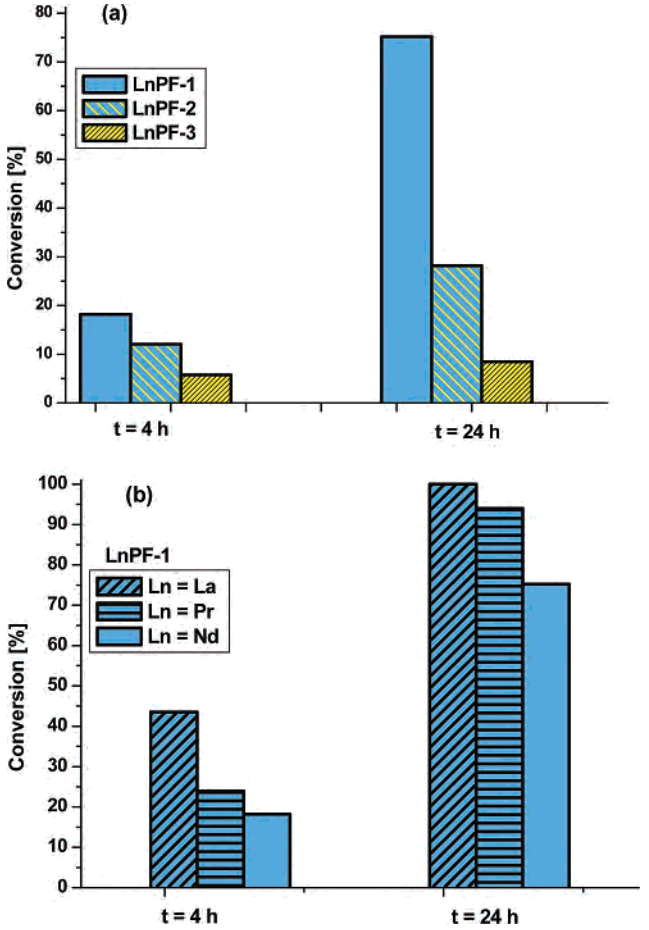

Figure 5. Catalytic oxidation of linalool: (a) activity of compounds LnPF-*n* ($n = 1-3$); (b) comparison of the catalytic activities in LnPF-1 materials (Ln = La, Pr, Nd).

Scheme 1

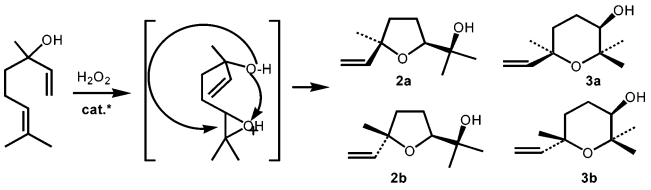

of the substrate to the metallic centers, the catalytic reactions thus taking place on the surface.

In a first stage, with the purpose of analyzing the coordination sphere influence in the catalyst behavior, only neodymium compounds were tested for the three families of compounds. Subsequently, to study the lanthanide influence in a same framework catalyst, LnPF-1 (Ln = Nd, La, and Pr) compounds were also comparatively tested, Figure 5.

Samples of LnPF-1 (Ln = La, Pr, Nd), LnPF-2, and LnPF-3 (Ln = Nd) were used as catalysts (0.021 mmol) for the transformation of linalool (330 mg, 2.1 mmol) by H_2O_2 (6.3 mmol) and MeCN (5 mL) in a glass reactor at 343 K. A series of blank experiments revealed that each component is essential for an effective catalytic reaction and the system is relatively unaffected by changing the order of mixing. The results show that catalysts LnPF-1 and LnPF-2 are active for the oxidation of linalool to hydroxy ethers (furanoid and pyranoid form) (**2**−**3**, Scheme 1), while LnPF-3 presents low

Table 3. Oxidation of Linalool with H_2O_2 Catalyzed by Different Nd−Sulfonates and Oxidation of Linalool with H_2O_2 Catalyzed by LnPF-1

Catalyzed by Different Nd−Sulfonates				
catalyst	conv (%) (h)	furans **2**	pyrans **3**	**2/3**
LnPF-1	76 (24)	52	23	2.3
LnPF-2	51 (48)	34.6	16.8	2.0
LnPF-3	17 (48)	11.5	5.2	2.2
Catalyzed by LnPF-1				
catalyst	conv (%) (h)	furans **2**	pyrans **3**	**2/3**
LnPF-1Nd	76 (24)	52	23	2.3
LnPF-1Pr	94 (22)	64.0	30.0	2.1
LnPF-1La	100 (22)	64.3	35.7	1.8

activity. All the catalysts are very selective, and no other reaction products were detected.

Looking at the results showed in Table 3, the following should be considered: (i) The 2:3 ratios found in all cases show that all materials behave similarly, indicating that they are produced by parallel reactions, through a common intermediate, and not by an isomerization process. It seems, thus, quite plausible that the process involves first the epoxidation at the metal site of the 2,3 double bond followed by the intramolecular opening of the epoxide ring by the hydroxy group at positions 6 or 7, the latter reaction being catalyzed by the acid sites. (ii) The LnPF-1 catalytic activity is the highest, followed by LnPF-2, with that of LnPF-3 being much lower. From the structural point of view, this behavior is directly related with the neodymium coordination number in each compound. This being 8 in LnPF-1, 8 and 9 in LnPF-2, and 9 in LnPF-3 gives rise to three different arrays involving the lanthanides, in their respective structures. The NdO_9 coordination in LnPF-3 makes it difficult to reach a higher coordination number during the catalytic reaction and explains its low activity. LnPF-1 and LnPF-2 exhibit 3D and 2D related structures, respectively. Although at first sight the 2D structure of LnPF-2 seems to be a better candidate, the fact of having one-half of the neodymium atoms nonacoordinated decreases its coordinative capability and, thus, the catalytic response. LnPF-1 having all Nd atoms octacoordinated offers the possibility of higher coordination during the catalytic process in all the active centers and drives the best results. (iii) Table 3 shows the results for Nd, Pr, and La compounds having the LnPF-1 structure type. In spite of the lack of porosity of this structure type, with, thus, the catalytic reaction being on surface, the activity of this family of catalysts is similar to that obtained when Ti-MCM-41 (yield: 80%) or Ti-Beta (yield: 73.4%) was used as catalyst.[26] The **2/3** ratios obtained using these catalysts (2.3−1.8) are much lower than the values obtained by the chemical routes described[27] (up to 9.0). The ratio values obtained with our catalyst are closer to that obtained when using epoxidase as catalyst[28] (∼1).

As expected, the lanthanide size influence is quite clear, with the best catalyst being the lanthanum compound,

(26) Schofield, L. J.; Kerton, O. J.; McMorn, P.; Bethell, D.; Ellwood, S.; Hutchings, G. J. *J. Chem. Soc., Perkin Trans.* **2002**, *2*, 1475−1481.
(27) Jpn. Kokai Tokkio Koho 59225176, 1984.
(28) di Stefano, R. *Bull. de L'O.J.V.* **1991**, 721.

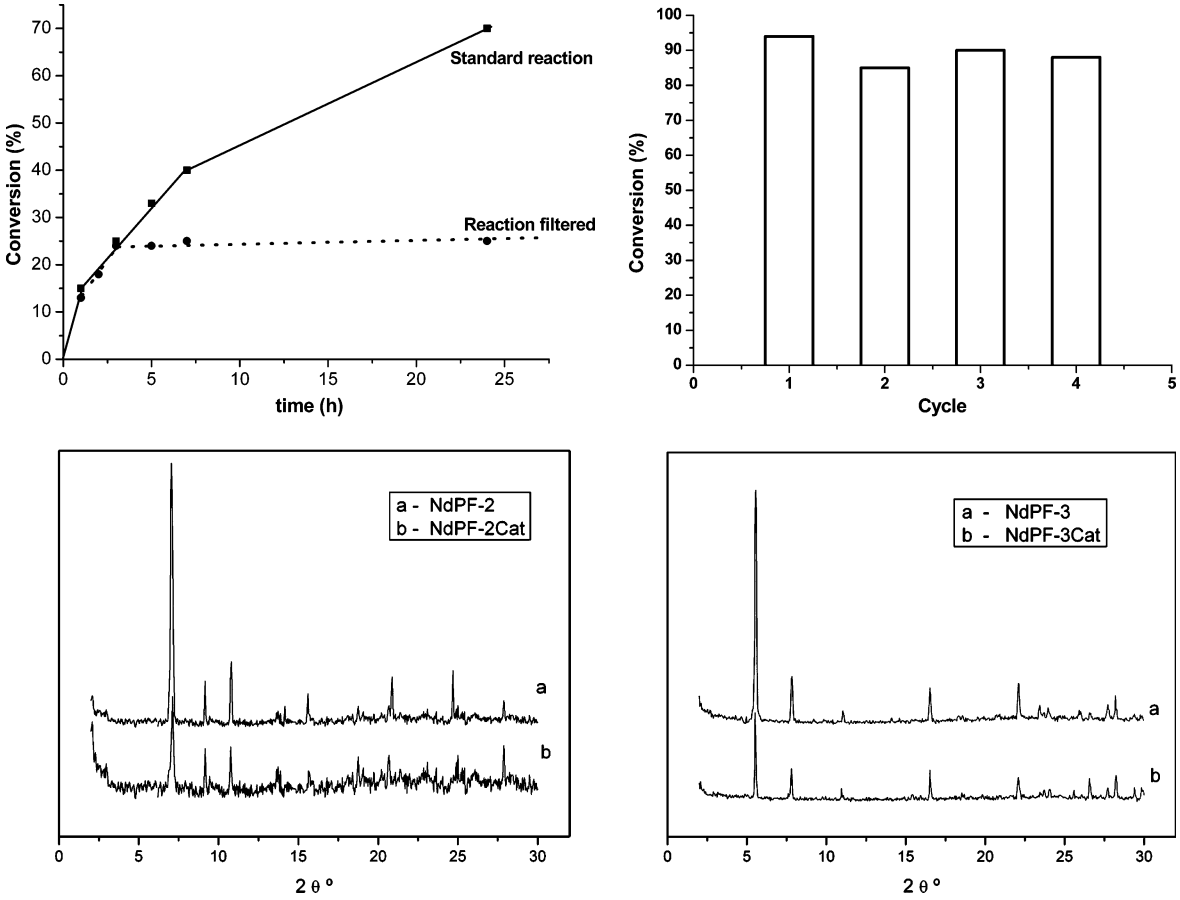

Figure 6. Top: Effect of removing the solid catalyst from the reaction (left) and recycling experiments for catalyst LnPF-1Pr (right). Bottom: Catalysts XRPD patterns before and after use.

followed by those of praseodymium and neodymium, corresponding to the decreasing value of their radii.

Separation, Recycling, and Catalyst Reuse. The major advantage of the use of heterogeneous catalysts is the ease with which they can be recovered from the reaction mixtures by simple filtration and reused.

The heterogeneous oxidation of linalool has been carried out until completeness. The five LnPF catalysts were filtered and washed, and then fresh substrate and solvent were added without further addition of catalyst, for four consecutive experiments, and both yield and activity were retained. In order to check the stability of the catalysts, we have characterized the solid before and after reaction (Figure 6). Although extensive studies have been carried out to elucidate the true catalytic species in the heterogeneous metal-catalyzed reaction, it is still unclear in many cases whether the reaction takes place on the surfaces of the solid catalyst or whether the active catalysts are M species solved out from the solid, which simply acts as a reservoir of metal. Taking this into account, it is mandatory to find out if some complex has passed into the solution. To do this, we have investigated the residual activity of the supernatant solution after separation of the catalyst. The potential leaching was studied as followed: the organic phase of a first run was separated from the solid (catalyst). New reagents were added to the clear filtrate, and the composition of the reaction mixture was determined by GC. This homogeneous reaction mixture was treated as a standard catalytic experiment. After 5 h, the composition was determined, and no reaction was observed, which excludes the presence of active species in solution.

Moreover, to rule out the contribution of homogeneous catalysis in the results shown in Table 3, one reaction was carried out in the presence of the solid until the conversion was ~20%, and at that point, the solid was filtered off at the reaction temperature. The liquid phase was transferred to another flask and again allowed to react, but no further significant conversion was observed (Figure 6, 23% after 24 h).[29]

An important point concerning the use of heterogeneous catalysts is its lifetime, particularly for industrial and pharmaceutical applications. After separation and washing, the heterogeneous catalysts were used several times for the same reaction under the same conditions as for the initial run of the catalyst. We usually see an increase of activity after the first run, followed by a slight decrease of the rate due to the small amount of catalyst lost by manipulation (Figure 6).

Magnetic Susceptibility Measurements. Figure 7 shows the plots of temperature dependence of the reciprocal molar magnetic susceptibility χ_m per Nd^{3+} mol in each LnPF formula for the three Nd materials. It can be observed that these magnetic susceptibilities present Curie−Weiss behavior

(29) Lempers, H. E. B.; Sheldon, R. A. *J. Catal*. **1998**, *175*, 62.

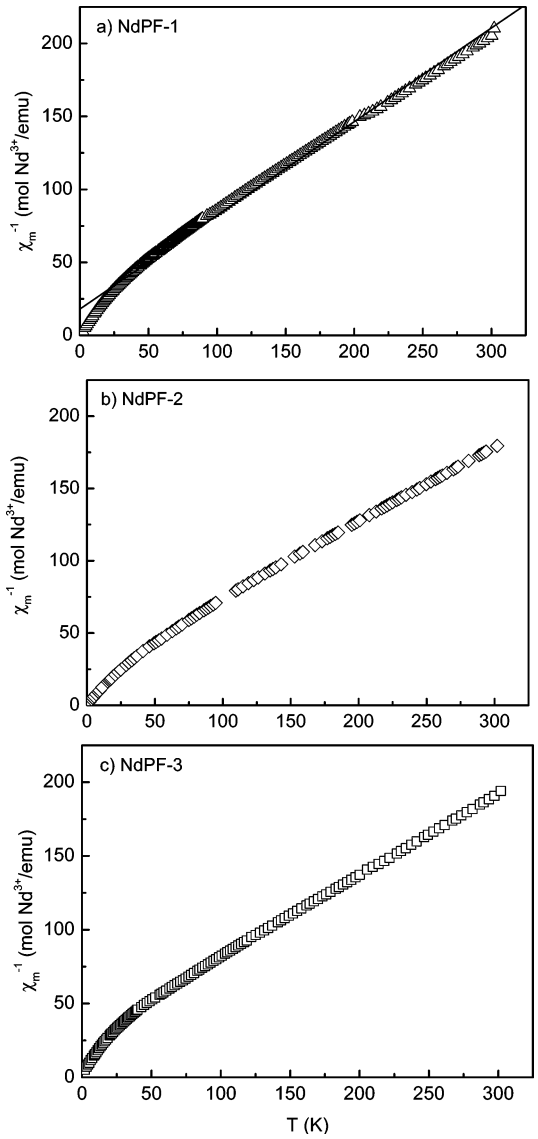

Figure 7. Plots of the reciprocal molar susceptibility (per Nd^{3+} mol in corresponding NdPF) as a function of temperature.

in a wide range of temperature, approximately above 40, 50, and 4−325 K, with expressions $\chi_m^{-1} = 18.1(6) + 0.642(4)\cdot T$ mol emu^{-1} ($r = 0.997$), $12.2(7) + 0.571(4)\cdot T$ mol emu^{-1} ($r = 0.997$), and $18.9(6) + 0.593(4)\cdot T$ mol emu^{-1} ($r = 0.997$), for NdPF-1, NdPF-2, and NdPF-3, respectively. Effective paramagnetic moments were determined to be 3.6, 3.8, and 3.7 μ_B, values which are very close to the expected value, 3.62 μ_B, for the Nd^{3+} free ion and comparable to the values commonly found in Nd compounds for which no magnetic interactions among cations exist. Therefore, observed downward deviations from the Curie−Weiss law below the indicated temperatures reflect only the splitting of the $^4I_{9/2}$ Nd^{3+} ground state under the influence of the crystal field (CF) in each case, and the Weiss constants $\theta = -28$, -21, and -32 K for NdPF-1, NdPF-2, and NdPF-3, respectively, are thus entirely due to CF effects.[30] Despite the existence of Nd-SBU giving rise to structural associations

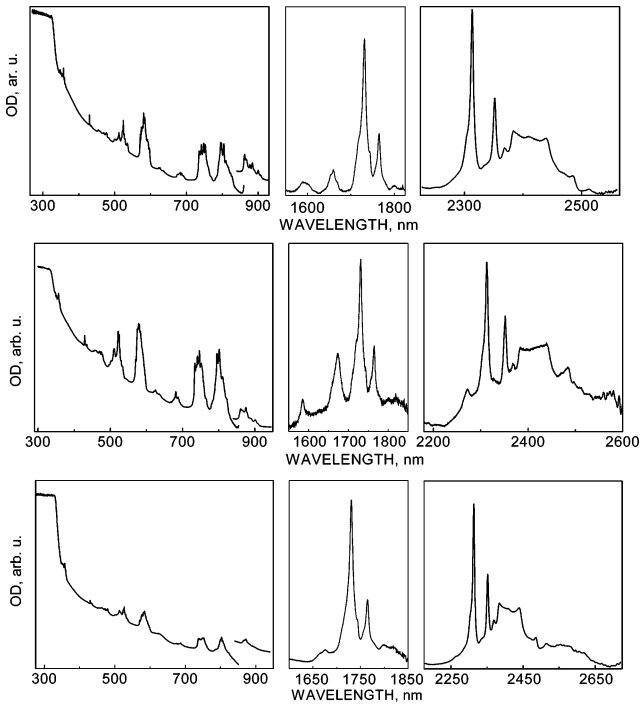

Figure 8. Room-temperature optical absorption spectra for NdPF-1 (top), NdPF-2 (middle), and NdPF-3 (bottom).

where Nd cations are at relatively short distances, the lack of observed three-dimensional Nd−Nd magnetic interaction is explained to be due to the behavior derived from the inner nature of 4f orbitals of Nd^{3+}, which do not favor the magnetic exchange, contrary to the observed situation in other lanthanide-containing structures including 3d cations, too. [21,31]

Optical Properties. Scarce research on the luminescent properties of rare earth purely sulfonate MOFs has been carried out to date,[13] although some study on mixed R-sulfonate−phosphonates has been conducted recently.[10] Focusing on optical applications and taking into account that polymer materials doped with rare earths are subjected to growing interest as low-cost alternatives to purely inorganic-based ones, mainly in optoelectronic devices as optical waveguides and optical waveguide amplifiers,[32] we are now attempting to give a general overview of room-temperature optical absorption and photoluminescence behavior of new rare earth coordination complexes.

Collected room-temperature optical absorption spectra of the three NdPF species consist of $^{2S+1}L_J$ Nd^{3+} multiplets ranging typically from ~2600 to 347 nm ($^4I_{13/2}$ up to $^4D_{1/2} + {}^2I_{11/2}$). The ultraviolet UV absorption edges, obtained from a linear extrapolation of the stepping absorption, are $\lambda_{th} =$ 338, 344, and 343 nm for NdPF-1, NdPF-2, and NdPF-3,

(30) Colón, C.; Medina, A.; Alonso; Fernández, F.; Sáez Puche, R.; Volkov, V.; Cascales, C.; Zaldo, C. *Chem. Mater.* **2005**, *17*, 6635.

(31) (a) Cascales, C.; Bucio, L.; Gutiérrez-Puebla, E.; Rasines, I.; Fernández Díaz, M. T. *Phys. Rev. B* **1998**, *57*, 5240. (b) Cascales, C.; Gutiérrez-Puebla, E.; Klimin, S.; Lebech, B.; Monge, M. A.; Popova, M. N. *Chem. Mater.* **1999**, *11*, 2520. (c) Cascales, C.; Fernández Díaz, M. T.; Monge, M. A. *Chem. Mater.* **2000**, *12*, 3369. (d) Cascales, C.; Monge, M. A.; Fernández Díaz, M. T.; Bucio, L. *Chem. Mater.* **2002**, *14*, 1995. (e) Sáez Puche, R.; Climent, E.; Romero de Paz, J.; Martinez, J. L.; Monge, M. A.; Cascales, C. *Phys. Rev. B* **2005**, *71*, 024403.

(32) Slooff, L. H.; van Blaaderen, A.; Polman, A.; Hebbink, G. A.; Klink, S. I.; Van Veggel, F. C. J. M.; Reinhoudt, D. N.; Hofstraat, J. W. *J. Appl. Phys.* **2002**, *91* (7), 3955.

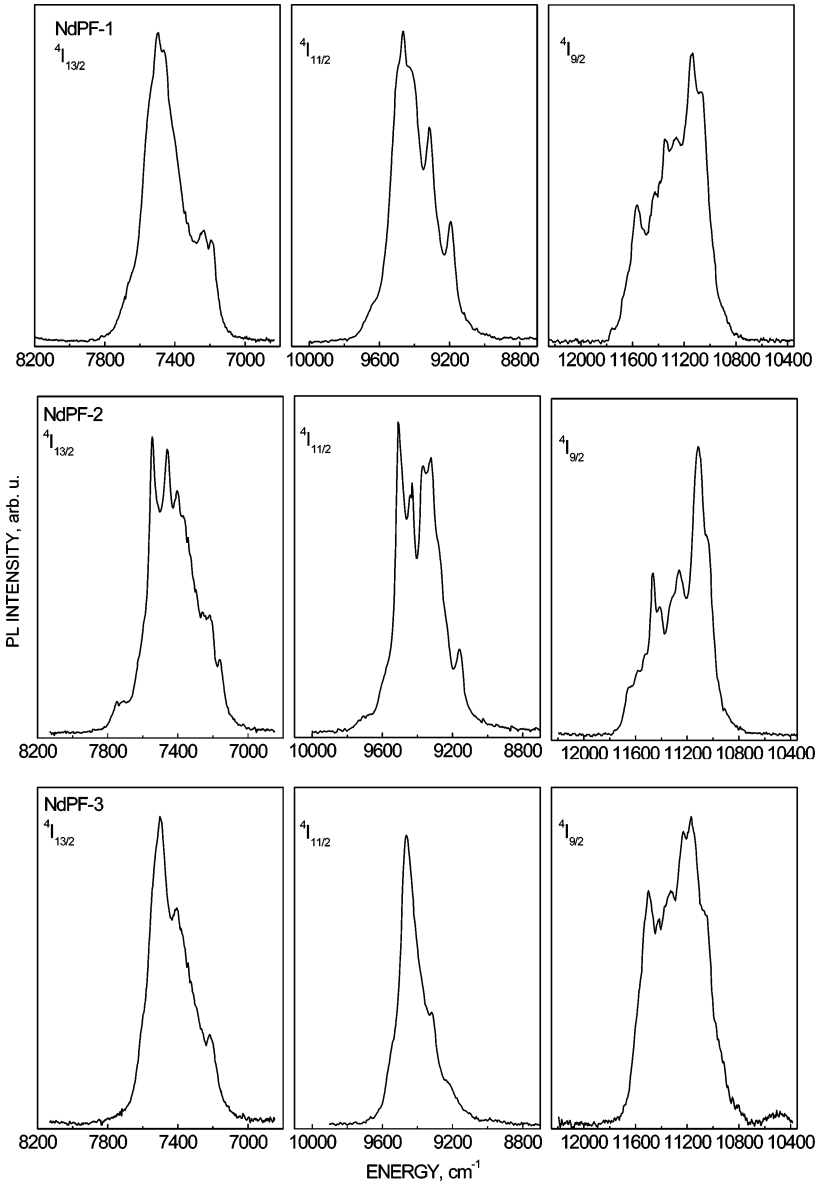

Figure 9. Room-temperature emission spectra from $^4F_{3/2}$ for NdPF-1, NdPF-2, and NdPF-3.

respectively, see Figure 8. Expected transitions, with origin in the Nd^{3+} ground state multiplet $^4I_{9/2}$, are clearly seen in these spectra. The transition from the lowest Stark component of $^4I_{9/2}$ to $^2P_{1/2}$, which can be used as an Nd^{3+} point site probe since it appears as a single peak for every independent Nd^{3+} crystal site in the current symmetries, presents the expected number of individual lines, 1, 4, and 3, for the above NdPF-1, NdPF-2, and NdPF-3 hosts. Positions of the most intense peak are significantly different, 23274, 23302, and 23254 cm^{-1}, respectively, which provide evidence for a clear nephelauxetic effect, and for the two Nd^{3+}-multicenter structures the difference between extreme high and low $^2P_{1/2}$ energies is from 312 cm^{-1} in PF-2 to 250 cm^{-1} in PF-3. The above higher $^2P_{1/2}$ separation value for PF-2 perfectly correlates with its observed wider distribution of Nd−O distances in the four coordination polyhedra, containing the shorter 2.243(8) and the larger 2.870(7) ones, thus yielding the more differentiated crystal field (CF) effects for this host. On the contrary, NdO_9 polyhedra in PF-3 are far more regular, and also similar among them, and consequently, their CF will be lesser different and somewhat smaller.[33]

Figure 9 gives the room-temperature PL spectra corresponding to $^4F_{3/2} \rightarrow {}^4I_{13/2}$, $^4I_{11/2}$, and $^4I_{9/2}$ transitions for the three Nd stoichiometric materials. Differences in these spectra arise from the particular distribution of emitting and final Stark energy levels of Nd^{3+} in every PF host. Because at room temperature photoluminescence from the two $^4F_{3/2}$ energy levels of each Nd^{3+} emitting center is expected, observed transitions to $^4I_{13/2}$, $^4I_{11/2}$, and $^4I_{9/2}$ consist of the corresponding overlapped bands, and no conclusions on the position and number of their energy levels can be extracted. Anyway, the above multiplets are split in all cases to the maximum number of crystal field levels, $2(J + {}^1/_2)$, by the low symmetry of Nd^{3+} centers in these PF hosts. Although the inherent uncertainty of optical measurements using

(33) Cascales, C.; Zaldo, C.; Sáez Puche, R. *Chem. Mater*. **2005**, *17*, 2052.

polycrystalline powders was considered, in order to compare their relative emission intensities the same weights of each sample were used in the prepared pellet, with the same pump laser power maintained during all experiments. The results indicate a better luminescence performance for Nd in PF-1 and PF-2 with regards to Nd in PF-3. Taking into account that from the corresponding crystallographic data the Nd^{3+} content per volume of PF unit cell can be calculated as 3.07×10^{-3}, 3.10×10^{-3}, and 4.32×10^{-3} $Å^{-3}$ for Nd stoichiometric PF-1, PF-2, and PF-3, respectively, it can be derived that nonradiative energy transfer losses can be greater in PF-3 for its highest Nd^{3+} concentration. Furthermore, along with the large amount of Nd^{3+} centers, the Nd backbone structural feature of PF-3, with the shortest 3.752(7) distance between Nd−Nd pairs, is also contributing to higher losses by cooperative excitation effects in the Nd stimulated emission process and some fluorescence lifetime reduction of the $^4F_{3/2}$ multiplet.

Conclusions

In summary, three families of multifunctional materials have been synthesized on the basis of different kinds of rare earth coordination polyhedra. The different geometry of the naphthalenedisulfonic acids used as linker [(1,5-NDS) and (2,6-NDS)] gives rise to the three new structure types. LnPF-1 and LnPF-2 (constitutional isomers, but with 3D and 2D structures, respectively) are the consequence of the sulfonate groups in different position in the NDS linker. LnPF-3 provide evidence that getting a 3D structure with 2,6-NDS is only possible with a greater Ln/linker ratio. It is worth pointing out the existence, in this latter family of compounds, of a μ^5-OH^- group, whose hydrogen atom is very close to one of the five coordinated Ln atoms (distance Ln···H = 2.09 Å).

These materials, with high thermal stability, act as active and selective bifunctional heterogeneous catalysts in oxidation of linalool yielding cyclic hydroxy ethers. Their activity depends more on the number of active centers with possibility of increasing the coordination number during the catalytic reaction, than on other structural effects, and, obviously, for the same structure type, on the rare earth size.

The absence of any three-dimensional Nd−Nd magnetic interaction is explained due to the inner nature of 4f orbitals of Nd^{3+}, which do not favor the magnetic exchange.

The influence of the PF matrix results in a better photoluminescence (PL) efficiency for NdPF-1, which moreover could be improved by exploring ways to reduce the PL quenching. This can be likely achieved by decreasing the Nd^{3+} concentration in the material, for instance, through the preparation, currently in progress, of mixed La/Nd compositions, since thus Nd−Nd interactions should lessen.

Acknowledgment. This work has been supported by the Spanish MCIT project MAT 2004-2001 and CTQ2004-02865/BQU. Consolider-ingenio 2010 CSD2006-0015.

Supporting Information Available: Crystallographic information (CIF). This material is available free of charge via the Internet at http://pubs.acs.org.

IC0617689